

# Enhanced Speciation of Pyrogenic Organic Matter from Wildfires Enabled by 21 T FT-ICR Mass Spectrometry

Holly K. Roth, Thomas Borch, Robert B. Young, William Bahureksa, Greg T. Blakney, Amelia R. Nelson, Michael J. Wilkins, and Amy M. McKenna\*



Cite This: *Anal. Chem.* 2022, 94, 2973–2980



Read Online

ACCESS |



Metrics & More

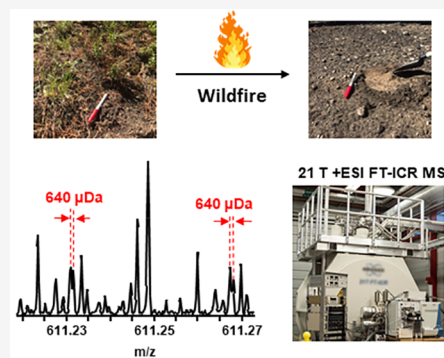


Article Recommendations



Supporting Information

**ABSTRACT:** Wildfires affect soils through the formation of pyrogenic organic matter (pyOM) (e.g., char and soot). While many studies examine the connection between pyOM persistence and carbon (C) composition, nitrogen (N) transformation in wildfire-impacted systems remains poorly understood. Thermal reactions in wildfires transform biomass into a highly complex, polyfunctional, and polydisperse organic mixture that challenges most mass analyzers. High-field Fourier transform ion cyclotron resonance mass spectrometry (FT-ICR MS) is the only mass analyzer that achieves resolving powers sufficient to separate species that differ in mass by the mass of an electron across a wide molecular weight range ( $m/z$  150–1500). We report enhanced speciation of organic N by positive-ion electrospray ionization (ESI) that leverages ultrahigh resolving power ( $m/\Delta m_{50\%} = 1\,800\,000$  at  $m/z$  400) and mass accuracy ( $<10$ – $100$  ppb) achieved by FT-ICR MS at 21 T. Isobaric overlaps, roughly the mass of an electron ( $M_e^- = 548$   $\mu\text{Da}$ ), are resolved across a wide molecular weight range and are more prevalent in positive ESI than negative ESI. The custom-built 21 T FT-ICR MS instrument identifies previously unresolved mass differences in  $\text{C}_c\text{H}_h\text{N}_n\text{O}_o\text{S}_s$  formulas and assigns more than 30 000 peaks in a pyOM sample. This is the first molecular catalogue of pyOM by positive-ion ESI 21 T FT-ICR MS and presents a method to provide new insight into terrestrial cycling of organic carbon and nitrogen in wildfire impacted ecosystems.



## INTRODUCTION

Forests provide a myriad of ecosystem services, including the storage of  $\sim 30$ – $40\%$  of terrestrial carbon (C),<sup>1</sup> but are highly susceptible to ecosystem disturbances (e.g., wildfires) that dramatically change foliage and landscape, and produce 256 Tg of pyrogenic C per year.<sup>2</sup> Although fires occur naturally across many ecosystems,<sup>3</sup> wildfire size, frequency, and severity has substantially increased in recent decades in forested ecosystems.<sup>4,5</sup> Incomplete combustion of soil organic matter (SOM) during wildfires forms byproducts (e.g., char and soot)<sup>6</sup> that can impact the quantity and quality of soil C and nitrogen (N).<sup>7,8</sup> Pyrogenic organic matter (pyOM) exists as a continuum that spans from macroscopic (i.e., char and soot) to microscopic scales (i.e., condensed polycyclic aromatic molecules)<sup>6</sup> across a range of physical and chemical properties. The composition of pyOM is determined by the type and amount of biomass and burn conditions (e.g., intensity, moisture, fuel density).<sup>9,10</sup> Collectively, pyOM is characterized by increased hydrophobicity, lower C/N ratios, coarser soil textures, increased pH, and higher electrical conductivity compared to nonfire impacted soil.<sup>9,11</sup>

Nitrogen is an essential and often limiting nutrient,<sup>12,13</sup> and inherent heating and postfire ecosystem dynamics change N lability and bioavailability.<sup>14,15</sup> In unburned/low temperature-impacted soils, N is in the form of a slightly acidic compound

(e.g., pyrrole, a ring structure composed of four C atoms and one N atom). As temperature increases, pyridinic structures (aromatic, basic functional groups) have been reported.<sup>16</sup> Although many studies focus on the connection between pyOM persistence and C composition,<sup>16</sup> there are limited reports on the connection between N composition and pyOM mineralization in fire-impacted soil.

The compositional complexity, polydispersity, and polyfunctionality of complex organic mixtures (SOM, pyOM, dissolved organic matter) challenge all analytical techniques. Fourier transform ion cyclotron resonance mass spectrometry (FT-ICR MS) routinely achieves resolving power sufficient to identify species that differ in mass by less than the mass of an electron, prevalent in natural organic matter (NOM).<sup>17–20</sup> The most widely used FT-ICR MS analytical approach for NOM combines solid-phase extraction (SPE) to enrich NOM from aqueous samples and negative-ion electrospray ionization (–ESI) to selectively ionize highly abundant carboxylic acids

**Received:** November 18, 2021

**Accepted:** January 12, 2022

**Published:** February 2, 2022



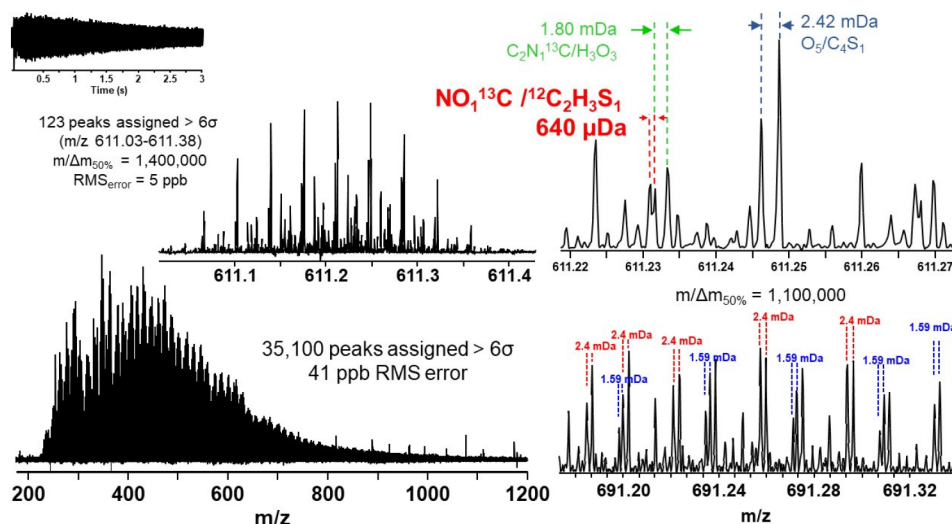


**Figure 1.** Positive-ion ESI 21 T FT-ICR mass spectrum of a pyOM extract. Bottom left: Broadband FT-ICR mass spectrum containing more than 35 000 assigned mass spectral peaks ( $m/z$  200–1200) with a root-mean-square mass error of 41 ppb, each with a signal magnitude greater than  $6\sigma$  of baseline noise, with  $m/\Delta m_{50\%} = 1\,800\,000$  at  $m/z$  400. Top left: 350 mDa mass scale-expanded segment, showing resolution of more than 120 mass spectral peaks at  $m/z$  611. Top right: mass scale-expanded segment across  $m/z$  691.1–691.4, showing the increase in the number of isobaric overlaps at higher  $m/z$ . Bottom right:  $\sim 60$  mDa mass scale-expanded segment, showing resolution of three isobaric overlaps: 2.42 mDa, 1.80 mDa, and 640  $\mu$ Da (mass of an electron is 548  $\mu$ Da).

in NOM.<sup>21</sup> However, studies that compare analyte selectivity in different ionization modes for pyOM remain limited.<sup>22,23</sup>

The first step in all mass spectral techniques is ionization to yield pseudomolecular ions, and it is selected on the basis of the analyte of interest. Negative-ion electrospray yields deprotonated molecular ions based on the ionization efficiency of acidic functional groups.<sup>22,24,25</sup> In  $-$ ESI, stronger acids are efficiently ionized,<sup>22</sup> and the most abundant peaks correspond to low  $pK_a$  carboxylic acids (see Table S1 for the  $pK_a$ 's of common soil functional groups), followed by phenolic groups that form as lignin degradation products.<sup>26</sup> Negative ESI is also sensitive to chemical contamination (i.e., linear alkylbenzene surfactants), which causes suppression of analyte ions and results in a mass spectrum dominated by chemical noise.<sup>27</sup> Ionization in  $-$ ESI is primarily dominated by low molecular weight carboxylic acids, and basic species and those with lower acidity can be detected by positive-ion ESI ( $+$ ESI). The  $pK_b$  distribution of basic functional groups in pyOM (e.g., pyridines and amides) results in less ion suppression due to more equal charge competition. Each ionization mode selectively ionizes a subset of species in a single SOM sample,<sup>28</sup> and no one soft ionization technique can equally access all of the compositional windows of SOM species. Ohno et al. benchmarked the field by comparing  $\pm$ ESI for unburned SOM and reported that the combination of elemental compositions from both modes increased the number of assignments by 43% compared to  $-$ ESI alone.<sup>21</sup> In addition, while other studies compare  $\pm$ ESI composition for soil- or water-derived SOM and refinery wastewater,<sup>21,29–31</sup> this study focuses on detailed characterization of pyOM, an understudied system in the field.

The unparalleled resolving power, high dynamic range, and increased sensitivity of the 21 T FT-ICR MS system identifies previously unresolved mass differences in  $C_cH_hN_nO_oS_s$  formulas within pyOM at high mass ranges ( $>m/z$  750).<sup>32,33</sup> The combination of high magnetic field, unique custom hardware, internal mass calibration, and absorption mode data processing available on the custom-built 21 T FT-ICR mass

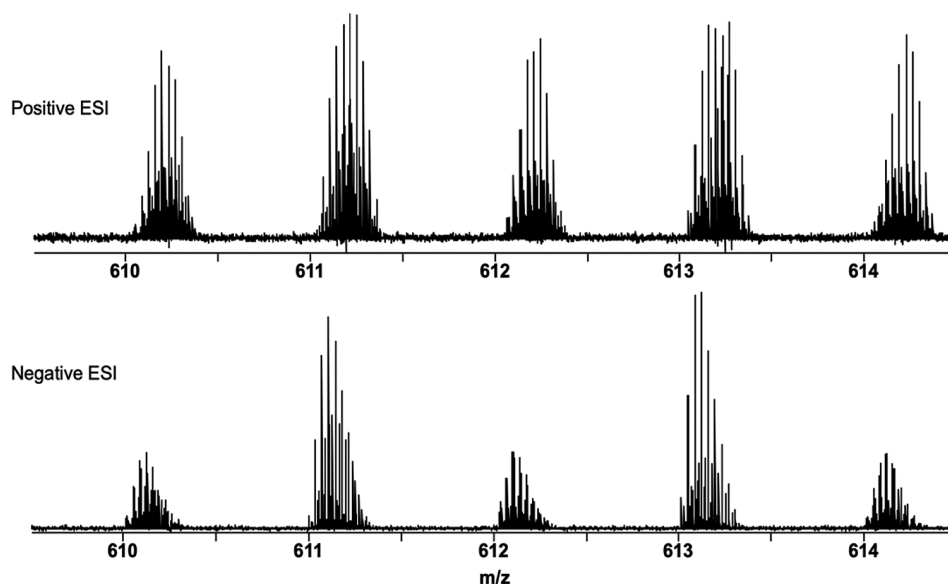
spectrometer achieves high resolving power ( $m/\Delta m_{50\%} = 2\,000\,000$  at  $m/z$  200), subppm mass accuracy (20–80 ppb), and high dynamic ranges that allow the assignment of more than 30 000 species in a single mass spectrum.<sup>32</sup> Here, we leverage the 21 T FT-ICR MS to illuminate the unique compositional window detected by  $+$ ESI, compare the same speciation to  $-$ ESI, and expand the compositional window of wildfire-impacted SOM. This is the first study to probe the molecular complexity of pyOM in positive-ion mode with 21 T FT-ICR mass spectrometry. We identify species that remain unresolved and thus undetected by lower resolution mass spectrometers and highlight the minimal resolving power requirements necessary to accurately assign elemental compositions. For the first time, more than 35 000 species are assigned at 30 ppb RMS error by  $+$ ESI 21 T FT-ICR MS, a new record for pyOM characterization.

## EXPERIMENTAL METHODS

**Soil Sampling and Preparation.** Soil was sampled in a lodgepole pine (*Pinus contorta*)-dominated region of the Medicine Bow National Forest, which burned in the 2018 Ryan fire. A high severity burned site was identified according to the amount of organic matter cover ( $<20\%$ ) and sampled from the organic horizon approximately one year after the fire's containment (for additional information, see Nelson et al.<sup>34</sup> (Sample # R89)). All solvents were HPLC grade and purchased from Sigma-Aldrich Chemical Co., St. Louis, MO, USA. Soil samples were weighed in acid-washed and combusted 250 mL Erlenmeyer flasks. A volume (in mL) of Milli-Q water twice the mass (in grams) was added to each flask and shaken (170 rpm for 10 h). Subsequently, the liquid was transferred into 50 mL centrifuge tubes and centrifuged for 10 min at 7500 rpm followed by filtering through a 0.2  $\mu$ m poly(ether sulfone) filter. 50 mL of each water sample was acidified to pH 2 with trace-metal grade HCl, followed by SPE with styrene-divinylbenzene (SDVB) polymer modified with a proprietary nonpolar surface (Bond Elut Priority Pollutant,

**Table 1. Isobaric Species Detected in pyOM by +ESI 21 T FT-ICR MS and Theoretical Resolving Power Required as a Function of Mass-to-Charge Ratio ( $m/z$ )**

	nominal mass (Da)	$\Delta$ exact mass (mDa)	$m/\Delta m_{50\%}$			
			$m/z$ 200	$m/z$ 400	$m/z$ 600	$m/z$ 800
$\text{NO}_2^{13}\text{C}/^{12}\text{C}_2\text{SH}_3$	59	0.640	310 000	625 000	930 000	1 200 000
$\text{C}_2\text{N}_1^{13}\text{C}/\text{H}_3\text{O}_3$	51	1.80	110 000	220 000	330 000	440 000
$\text{O}_5/\text{C}_4\text{S}_1$	80	2.40	83 000	160 000	250 000	330 000
$\text{CN}_4/\text{H}_4\text{O}_4$	68	1.35	150 000	290 000	440 000	590 000

**Figure 2.** Mass-scale expanded zoom insets for +ESI (top) and –ESI (bottom) across  $m/z$  609.5–614.5 of a pyOM extract.

Agilent Technologies).<sup>29</sup> Water-soluble organics were eluted with HPLC grade methanol and stored in precombusted glass vials at 4 °C in the dark prior to analysis.

**21 T FT-ICR Mass Spectrometry.** Ions were generated at atmospheric pressure via a microelectrospray source<sup>35</sup> and analyzed by 21 T FT-ICR MS.<sup>32,33</sup> Peaks with signal magnitude greater than 6 times the baseline root-mean-square (RMS) noise at  $m/z$  500 were exported to peak lists, phase-corrected,<sup>36</sup> and internally calibrated on the basis of the “walking” calibration method.<sup>37</sup> Molecular formula assignments were performed with PetroOrg software.<sup>38</sup> Complete experimental details can be found in the [Supporting Information](#). All FT-ICR mass spectra files and assigned elemental compositions are publicly available via the Open Science Framework at <https://osf.io/758ux/> (DOI: 10.17605/OSF.IO/758UX).

## RESULTS AND DISCUSSION

**Positive ESI 21 T FT-ICR MS of pyOM Identifies New Isobaric Overlaps.** Figure 1 shows the broadband +ESI FT-ICR mass spectrum for a pyOM extract with more than 35 000 assigned mass spectral peaks (signal magnitude of six times greater than the baseline noise level) between  $m/z$  200 and 1300, centered at  $m/z$  480 (bottom left). The achieved resolving power ( $m/\Delta m_{50\%}$ , in which  $\Delta m_{50\%}$  is the mass spectral peak full width at half-maximum peak height)<sup>17</sup> is 1 800 000 at  $m/z$  400, which enables resolution and assignment of 35 100 peaks at a root-mean-square error of 41 ppb. The mass scale-expanded segment at  $m/z$  611 highlights the immense spectral density with  $\sim$ 123 peaks within a 0.3 mDa

window assigned with a RMS error of 5 ppb (Figure 1 (top left)). The theoretical resolving power required to separate equally abundant species that differ in mass by  $\sim$ 640  $\mu$ Da at  $m/z$  600 is 950 000. Here, the achieved resolving power ( $m/\Delta m_{50\%} = 1\,400\,000$  at  $m/z$  611) enables the separation of species with the same nominal mass (59 Da) that differ in exact mass by 640  $\mu$ Da ( $\text{NO}_2^{13}\text{C}$  versus  $^{12}\text{C}_2\text{SH}_3$ ), approximately the mass of an electron (548  $\mu$ Da).<sup>39–41</sup> Table 1 shows isobaric overlaps and minimum achieved resolving power requirements for equally abundant species in pyOM samples by +ESI. Importantly, resolving power requirements will exceed the minimum for species of varying abundances.<sup>17,42,43</sup>

The polyfunctionality and polydispersity in molecular composition and structure of pyOM systems results in a highly complex mass spectrum for all ionization modes, including –ESI. Figure S1 shows the –ESI 21 T FT-ICR mass spectrum with more than 32 000 acidic species assigned between  $m/z$  200 and 1000 with the mass distribution centered at  $m/z$   $\sim$  375 (Figure S1 (bottom left)). Negative-ion ESI remains dominated by carboxylic acid moieties, yet still results in a highly complex mass spectrum. The mass scale-expanded segment at  $m/z$  611 shows 66 peaks assigned with a RMS error of 7 ppb (Figure S1 (top left)) and highlights the mass spectral complexity in –ESI. However, comparison of the same nominal mass range shows that +ESI detects more than twice the number of peaks (123 peaks) compared to –ESI (66 peaks) and illustrates the dominance of carboxylic acid ionization in negative-ion mode. Improved speciation of pyOM, especially lower abundant species, requires more than

one ionization mode to more accurately identify compositional trends across a wide molecular weight range.

**Ionization Efficiency: +ESI vs –ESI.** Efficient ionization of  $O_x$  species in –ESI can be rapidly visualized when compared to +ESI for the same sample across the same narrow mass range. Figure 2 shows mass-scale expanded zoom insets for +ESI (top) and –ESI (bottom) across  $m/z$  609.5–614.5. Species in both spectra are composed of singly charged species based on the unit  $m/z$  separation between  $^{12}C_n$  and  $^{13}C_1^{12}C_{n-1}$  isotopic variants of the same elemental composition.<sup>44</sup> The most abundant peaks in positive and negative mode correspond to odd nominal mass species (e.g.,  $m/z$  611 and 613). Mass spectral peaks with the highest signal magnitude detected by –ESI correspond to  $O_x$  species at odd nominal mass and  $^{13}C_1O_x$  at even nominal mass.<sup>45</sup> Conversely, +ESI across the same mass window shows approximately equal signal magnitude for even and odd nominal mass species and results in the detection of twice as many species. This is likely due to a combination of the narrow range of basicity in SOM compared to acidity and the relative concentrations of basic functional groups, which leads to more equal ionization in +ESI.

Tables S2 and S3 show  $m/z$ , mass error, resolving power, signal-to-noise ratio (S/N), double-bond equivalent (DBE), and neutral elemental composition for all mass spectral peaks detected above  $6\sigma$  at  $m/z$  611 and 612 by +ESI (Table S2) and –ESI (Table S3). Across the 348 mDa region, >120 peaks are assigned elemental compositions with a RMS mass error of 6 ppb by +ESI (Table S2a) compared to 66 peaks across a similar mass range (RMS error of 6 ppb, error plot in Figure S3) by –ESI for the same sample. The shift of one nominal mass unit higher across each spectrum to  $m/z$  612 (Tables S2b and S3b) shows a similar trend with 96 peaks assigned at a RMS error of 5 ppb by +ESI (across 312 mDa) compared to 54 peaks at a 9 ppb RMS error by –ESI (285 mDa). Positive ESI contains more isobaric species with tighter mass differences (1.59 mDa), which are resolved by 21T FT-ICR MS (Table 1). Additionally, +ESI identifies more N species (56 at  $m/z$  611 and 67 at  $m/z$  612) compared to –ESI (25 at  $m/z$  611 and 31 at  $m/z$  612) and further highlights the increased compositional coverage for +ESI compared to –ESI for pyOM.

**Positive-Ion ESI Identifies 12 475 Unique Species Not Observed in Negative-Ion ESI.** The differences in spectra result in detection of unique species by each ionization mode, shown in Table 2. Positive ESI results in 24 189 formulas compared to 11 301 by –ESI, a more than 2-fold increase in identified species. Removal of the sodiated adducts from +ESI

reduces the number of formulas assigned to 21 010 (only the CHO species resulted in sodiated adducts). For simplicity, further discussion of the elemental assignments will be limited to the nonsodiated fraction. Between –ESI and +ESI, there are 8535 formulas in common to both modes, 4371 CHO and 4164 CHNO, which comprise nearly all the –ESI assignments. Stated another way, ~76% of the total –ESI formulas and nearly 86% and 91% of the CHO and CHNO are also detected by +ESI. However, common assignments represent only ~41% of the assignments by +ESI (~65% of CHO and ~30% of CHNO).

The unique formulas assigned for each mode were determined by eliminating neutral elemental compositions assigned in both spectra. However, it is important to note that it is possible that structural isomers may be present that have the same elemental composition and thus cannot be differentiated by mass alone. For unique CHO species, only 741 species were assigned in negative mode, whereas 2361 species were assigned in positive mode. However, for CHNO species, 9851 unique species were assigned by +ESI compared to only 404 unique formulas in –ESI, an increase of ~87% and more than twice the number previously reported.<sup>21</sup> Out of 21 010 nonsodiated species assigned in positive-ion mode, 12 475 are unique; put generally, +ESI displays more unique formulas than it has in common with negative-ion mode. Thus, the use of +ESI identifies organic N species in pyOM that remain undetected by –ESI and results in an expansion of the analytical window into complex fire-impacted systems.

**Chemical Properties Are Influenced by Ionization Limitations.** Chemical property calculations from elemental compositions detected by FT-ICR MS analysis are common in NOM systems for the rapid identification of qualitative trends between samples. For example, the nominal oxidation state of carbon (NOSC) describes a molecule's lability because it is directly related to the Gibbs free energy ( $\Delta G^\circ$ ) of the reduction half-reaction between organic matter as the electron donor and the available terminal electron acceptor (e.g., oxygen) (eq S1).<sup>46</sup> However, calculated properties based on elemental compositions will change based on the number and type of species detected. Table S4 shows average H/C, O/C, N/C, NOSC, and double-bond equivalents (DBEs) (eq S2), plus the average C, H, O, and N number per formula, for both  $\pm$ ESI spectra. For both polarities, the H/C ratio is ~1 with ~10 more C and 12 more H in +ESI than in –ESI. The average number of oxygens is 1.3 higher in –ESI, in agreement with Hertkorn et al.,<sup>47</sup> due to the preferential ionization of O-rich molecules. The differences in average C, H, and N are propagated by differences in DBE, which is four units higher for +ESI, demonstrating how the differences in species detected are propagated through calculated indices. Finally, the distribution of the NOSC assignments displays a distinct shift toward higher oxidation and lower C number in the –ESI sample (Figure S3 (top)). This shift is even more distinct in the CHNO class (Figure S3 (bottom)), which shows a shift toward lower, more reduced NOSC values in +ESI. Together, these properties clearly demonstrate that any calculation based on elemental composition must be evaluated with caution.

**Positive ESI at 21 T FT-ICR MS Resolves and Identifies Dissolved Organic Nitrogen.** Compared to –ESI, +ESI more efficiently ionizes N-containing species (Table 2). Figure S4 shows the heteroatom class distribution comparison for the same sample of pyOM by  $\pm$ ESI (see Figure S5 for relative abundances). Nitrogen species detected by +ESI contain a

**Table 2. Formula Assignments and Elemental Class Distributions of the CHO and CHNO Fractions of the Negative-Ion and Positive-Ion ESI Spectra of a pyOM Extract**

	$\pm$			common
	–ESI	+ESI	+ESI (no Na)	
formulas assigned	11 301	24 189	21 010	8535
unique formulas	2766	15 654	12 475	N/A
CHO	5112	9911	6732	4371
unique CHO	741	5540	2361	N/A
CHNO	4568	14 015	14 015	4164
unique CHNO	404	9851	9851	N/A

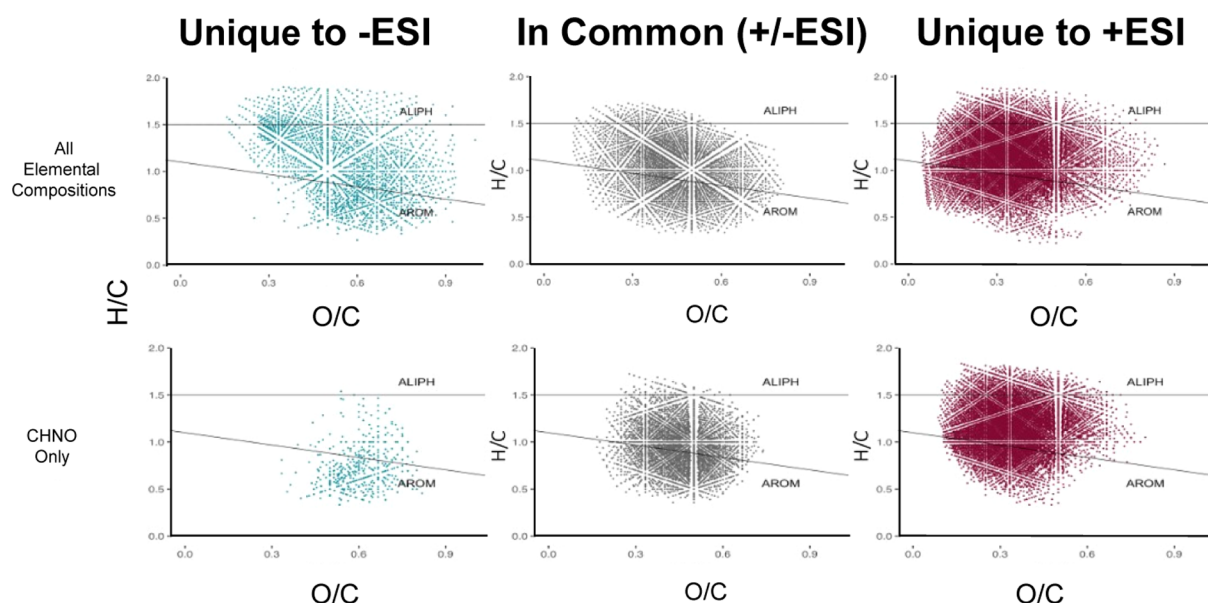


**Figure 3.** Top: van Krevelen diagrams of all the assigned formulas of the pyOM extract. Bottom: van Krevelen diagrams of only the CHNO class assignments. Unique formulas assigned for  $-ESI$  are on the left (blue); formulas in common are in the middle (gray), and formulas unique to  $+ESI$  are on the right (red).

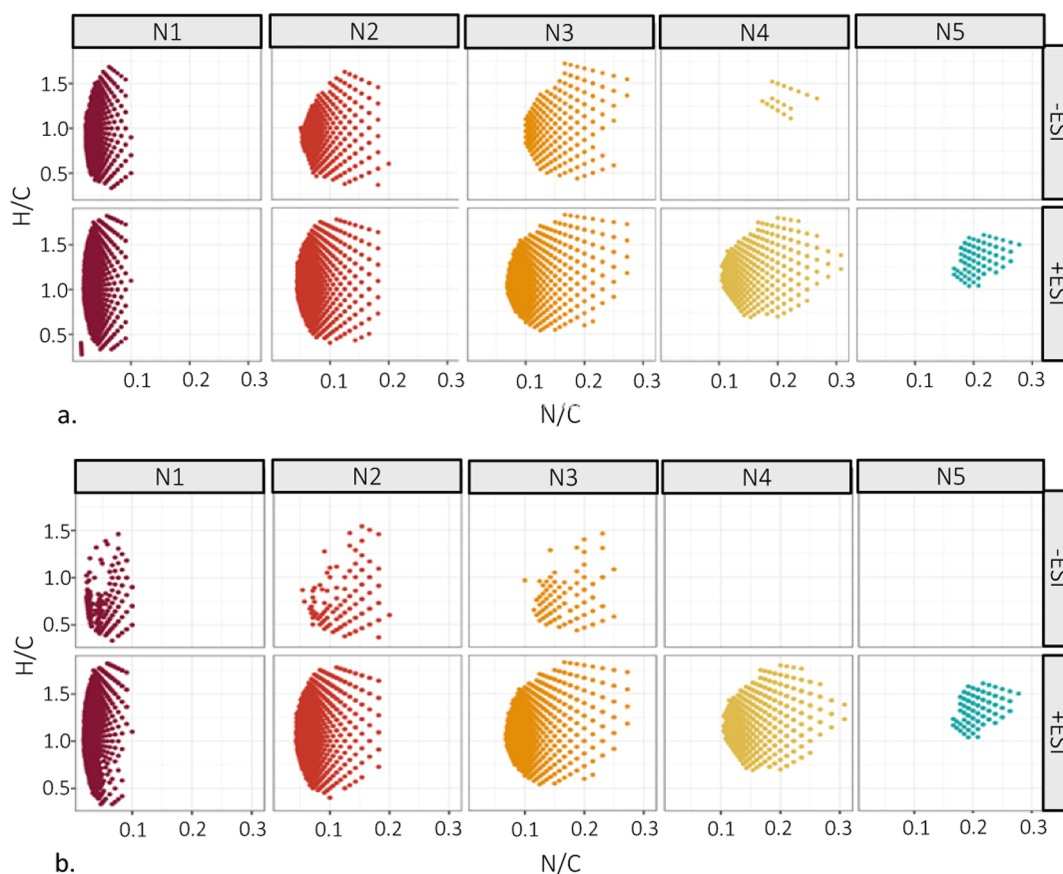


**Figure 4.** Atomic H/C vs N/C ratios of neutral species detected in a pyOM extract. (a) All CHNO assigned,  $-ESI$  assignments on the top row and  $+ESI$  assignments on the bottom row. (b) Only the unique CHNO assigned, again with  $-ESI$  on the top row and  $+ESI$  on the bottom row. Both panels are separated by N number, which increases from left to right.

higher number of N atoms per molecule (i.e.,  $N_3$ ,  $N_4$ , and  $N_5$ ), likely composed of a range of basic functionalities (e.g., pyridines and amides). Species with high N substitution (e.g.,  $N_5$ ) are not detected in  $-ESI$ . Additionally,  $+ESI$  identifies a

higher number of low oxygen-number classes (e.g.,  $O_2$  and  $O_3$ ). In fact, six  $CHN_1$  classes were assigned in  $+ESI$ , in addition to  $CHN_1O_2$ ,  $CHN_2O_{2-3}$ ,  $CHN_3O_{2-4}$ ,  $CHN_4O_{4-6}$ , and all  $CHN_5O_x$  that were not detected by  $-ESI$ . This suggests

that speciation and molecular detection of dissolved organic N in SOM systems could be significantly improved by 21 T FT-ICR MS in positive-ion mode.

**Van Krevelen Diagrams Highlight the Increased Compositional Coverage of +ESI at 21 T.** van Krevelen diagrams plot the H/C ratio versus the O/C ratio of neutral species, and different regions of the H/C and O/C space correspond to the molar ratios of major biogeochemical precursors (e.g., lignin-like, peptide-like, and lipid-like).<sup>48</sup> Because FT-ICR MS results in tens of thousands of elemental compositions in a single mass spectrum, van Krevelen diagrams are widely applied to rapidly visualize compositional changes between samples.<sup>49</sup> Figure 3 (top) shows van Krevelen diagrams derived from both ionization modes for all assigned species. Elemental compositions unique to –ESI are shown in blue (left); those identified in both spectra are in gray (middle), and species unique to +ESI are shown in red (right). Unique species in –ESI primarily have an O/C between 0.3 and 0.9, whereas species unique to +ESI have an O/C spanning 0.1 to 0.9. As shown in Table 2, 2766 formulas are unique to –ESI and 12 475 are unique to +ESI. These species span similar compositional ranges but are lower in total number of species in –ESI.

**Unique Compositional Space of Nitrogen Species by +ESI 21 T FT-ICR MS.** Figure 3 (bottom) shows van Krevelen diagrams for unique N-containing species by  $\pm$ ESI. Importantly, across a wide range of H/C and O/C, positive-ion mode species occupy a much more diverse compositional range compared to –ESI with only 404 peaks in –ESI compared to 9851 peaks in +ESI (more than 24 $\times$  the formula assignments in –ESI) (Table 2). These figures demonstrate that, across a wide range of compositional and structural classes, +ESI identifies a wide range of N species. Importantly, species that correspond to H/C ratios >1.0 and O/C ratios >0.3 are uniquely detected by +ESI and remain undetected by –ESI. This region of van Krevelen space (H/C > 1.0 and O/C > 0.35) has previously been reported as an indicator for the presence of potential toxicants due to the inhibition of aquatic photosynthetic organisms.<sup>50</sup> Therefore, the characterization of pyOM by +ESI identifies potentially toxic species not detected by –ESI. Differences in the O/C ratio are illustrated in Figure S6, which shows that –ESI identifies more species with a high oxygen content, while +ESI can more efficiently ionize those with a lower oxygen content.

**Modified van Krevelen Diagrams: H/C versus N/C.** A useful complement to the traditional van Krevelen diagram is the H/C vs N/C plot, shown for the total assigned CHNO fraction (Figure 4a) and the unique CHNO assignments (Figure 4b). Each panel is further divided by ionization mode (–ESI on top) and N number (1–5 from left to right). The compositional space for the total assigned species spans similar compositional ranges for N<sub>1</sub> (N/C > 0.1) and N<sub>2</sub> (N/C > 0.2) species but becomes more evident for N<sub>3</sub>–N<sub>5</sub> with only 25 N<sub>4</sub> species identified by negative-ion mode and no N<sub>5</sub> species detected (Figure 4a). For the unique formula assignments, the difference in N/C spans across all N classes. For N<sub>1–3</sub>, the unique formulas in negative-ion mode are clustered toward lower H/C ratios (H/C < 1.0), while N<sub>4</sub> and N<sub>5</sub> do not display any unique formulas (Figure 4b), further highlighting the increased speciation of CHNO by positive-ion mode. Thus, for research that is focused on changes in N content, +ESI should be utilized as the preferred method. Importantly, previous studies utilizing both negative and positive ESI were not able

to provide the level of resolution for the nitrogenated molecules that we report here.<sup>21,23,47</sup> Therefore, this key element for microbial processing and ecosystem productivity is relatively understudied within the field of FT-ICR MS.

## CONCLUSIONS

21 T FT-ICR MS in +ESI displayed clear shifts in pyOM composition compared to –ESI, highlighting differences in the ionization mechanism that proliferate into the resulting spectrum. The addition of +ESI resulted in an 87% increase (12 475 additional formulas) in the nonsodiated species compared to the traditional –ESI-only analysis. This included 9851 unique CHNO formulas, which spanned a wider compositional range, and demonstrated that a large fraction of organic N is overlooked with analysis only by –ESI. Additionally, it was shown that the biases associated with calculating chemical parameters by any ionization mechanism (e.g., NOSC) must be fully understood for proper use in C and N cycling models. Finally, while no one ionization mode can address the complexity of SOM, the combination of ESI in positive- and negative-ion modes substantially expands the analytical window for fire-impacted systems.

## ASSOCIATED CONTENT

### Supporting Information

The Supporting Information is available free of charge at <https://pubs.acs.org/doi/10.1021/acs.analchem.1c05018>.

Data tables (ZIP)

Additional experimental details, peak lists, FT-ICR MS spectra and error plots, calculated chemical parameters, and FT-ICR MS images (PDF)

## AUTHOR INFORMATION

### Corresponding Author

Amy M. McKenna – National High Magnetic Field Laboratory, Ion Cyclotron Resonance Facility, Florida State University, Tallahassee, Florida 32310-4005, United States; Department of Soil and Crop Sciences, Colorado State University, Fort Collins, Colorado 80523-1170, United States; [orcid.org/0000-0001-7213-521X](https://orcid.org/0000-0001-7213-521X); Phone: +1 850 644 4809; Email: [mckenna@magnet.fsu.edu](mailto:mckenna@magnet.fsu.edu); Fax: +1 850 644 1366

### Authors

Holly K. Roth – Department of Chemistry, Colorado State University, Fort Collins, Colorado 80523, United States; [orcid.org/0000-0003-2733-517X](https://orcid.org/0000-0003-2733-517X)

Thomas Borch – Department of Chemistry, Colorado State University, Fort Collins, Colorado 80523, United States; Department of Soil and Crop Sciences, Colorado State University, Fort Collins, Colorado 80523-1170, United States; [orcid.org/0000-0002-4251-1613](https://orcid.org/0000-0002-4251-1613)

Robert B. Young – Chemical Analysis & Instrumentation Laboratory, New Mexico State University, Las Cruces, New Mexico 88003, United States; [orcid.org/0000-0001-7485-0604](https://orcid.org/0000-0001-7485-0604)

William Bahureksa – Department of Chemistry, Colorado State University, Fort Collins, Colorado 80523, United States

Greg T. Blakney – National High Magnetic Field Laboratory, Ion Cyclotron Resonance Facility, Florida State University, Tallahassee, Florida 32310-4005, United States; [orcid.org/0000-0002-4205-9866](https://orcid.org/0000-0002-4205-9866)

Amelia R. Nelson – Department of Soil and Crop Sciences, Colorado State University, Fort Collins, Colorado 80523-1170, United States

Michael J. Wilkins – Department of Soil and Crop Sciences, Colorado State University, Fort Collins, Colorado 80523-1170, United States

Complete contact information is available at:

<https://pubs.acs.org/10.1021/acs.analchem.1c05018>

## Notes

The authors declare no competing financial interest.

## ACKNOWLEDGMENTS

The authors thank Christopher L. Hendrickson, Chad R. Weisbrod, and John P. Quinn for the design and maintenance of the 21 T instrument. This work was supported by NSF Division of Chemistry and Division of Materials Research through DMR-1644779 and the State of Florida. The authors also acknowledge support to T.B. from the National Science Foundation under Grant Number 1512670 and USDA National Institute of Food Agriculture through AFRI grant no. 2021-67019034608. This research was funded by the National Science Foundation (2114868) and AFRI grant no. 2021-67019-33726 from the USDA National Institute of Food and Agriculture.

## REFERENCES

- (1) Bladon, K. D.; Emelko, M. B.; Silins, U.; Stone, M. *Environ. Sci. Technol.* **2014**, *48* (16), 8936–8943.
- (2) Jones, M. W.; Santín, C.; van der Werf, G. R.; Doerr, S. H. *Nat. Geosci.* **2019**, *12* (9), 742–747.
- (3) Giglio, L.; Randerson, J. T.; van der Werf, G. R. *J. Geophys. Res. Biogeosci.* **2013**, *118* (1), 317–328.
- (4) Abatzoglou, J. T.; Williams, A. P. *Proc. Natl. Acad. Sci. U.S.A.* **2016**, *113* (42), 11770–11775.
- (5) Dennison, P. E.; Brewer, S. C.; Arnold, J. D.; Moritz, M. A. *Geophys. Res. Lett.* **2014**, *41* (8), 2928–2933.
- (6) Bird, M. I.; Wynn, J. G.; Saiz, G.; Wurster, C. M.; McBeath, A. *Annu. Rev. Earth and Planet. Sci.* **2015**, *43*, 273–298.
- (7) González-Pérez, J. A.; González-Vila, F. J.; Almendros, G.; Knicker, H. *Environ. Int.* **2004**, *30* (6), 855–870.
- (8) Knicker, H. *Biogeochemistry* **2007**, *85* (1), 91–118.
- (9) Viedma, O.; Quesada, J.; Torres, I.; de Santis, A.; Moreno, J. M. *Ecosystems* **2015**, *18* (2), 237–250.
- (10) Pierson, D. N.; Robichaud, P. R.; Rhoades, C. C.; Brown, R. E. *Int. J. Wildland Fire* **2019**, *28* (10), 814–821.
- (11) Santín, C.; Doerr, S. H.; Kane, E. S.; Masiello, C. A.; Ohlson, M.; de la Rosa, J. M.; Preston, C. M.; Dittmar, T. *Glob. Change Biol.* **2016**, *22* (1), 76–91.
- (12) Geisseler, D.; Horwath, W. R.; Joergensen, R. G.; Ludwig, B. *Soil Biol. Biochem.* **2010**, *42*, 2058–2067.
- (13) Acquisti, C.; Elser, J. J.; Kumar, S. *Mol. Biol. Evol.* **2009**, *26* (5), 953–956.
- (14) Adkins, J.; Sanderman, J.; Miesel, J. *Geoderma* **2019**, *333*, 10–22.
- (15) Miesel, J. R.; Hockaday, W. C.; Kolka, R. K.; Townsend, P. A. *J. Geophys. Res. G: Biogeosci.* **2015**, *120* (6), 1124–1141.
- (16) Torres-Rojas, D.; Hestrin, R.; Solomon, D.; Gillespie, A. W.; Dynes, J. J.; Regier, T. Z.; Lehmann, J. *Geochim. Cosmochim. Acta* **2020**, *276*, 170–185.
- (17) Marshall, A. G.; Hendrickson, C. L.; Jackson, G. S. *Mass Spectrom. Rev.* **1998**, *17*, 1–35.
- (18) Stubbins, A.; Spencer, R. G. M.; Chen, H.; Hatcher, P. G.; Mopper, K.; Hernes, P. J.; Mwamba, V. L.; Mangangu, A. M.; Wabakanghanzi, J. N.; Six, J. *Limnol. Oceanogr.* **2010**, *55* (4), 1467–1477.
- (19) Kujawinski, E. B.; del Vecchio, R.; Blough, N. v.; Klein, G. C.; Marshall, A. G. *Mar. Chem.* **2004**, *92*, 23–37.
- (20) Dittmar, T.; Koch, B. P. *Mar. Chem.* **2006**, *102* (3–4), 208–217.
- (21) Ohno, T.; Sleighter, R. L.; Hatcher, P. G. *Anal. Bioanal. Chem.* **2016**, *408* (10), 2497–2504.
- (22) Krueve, A.; Kaupmees, K.; Liigand, J.; Leito, I. *Anal. Chem.* **2014**, *86* (10), 4822–4830.
- (23) Hockaday, W. C.; Purcell, J. M.; Marshall, A. G.; Baldock, J. A.; Hatcher, P. G. *Limnol. Oceanogr.: Methods* **2009**, *7* (1), 81–95.
- (24) Whitehouse, C. M.; Dreyer, R. N.; Yamashita, M.; Fenn, J. B. *Anal. Chem.* **1985**, *57* (3), 675–679.
- (25) Fenn, J. B.; Mann, M.; Meng, C. K.; Wong, S. F.; Whitehouse, C. M. *Science* **1989**, *246* (4926), 64–71.
- (26) Qi, Y.; Fu, P.; Volmer, D. A. *Mass Spectrom. Rev.* **2020**, DOI: 10.1002/mas.21634.
- (27) Young, R. B.; Avneri-Katz, S.; McKenna, A. M.; Chen, H.; Bahureksa, W.; Polubesova, T.; Chefetz, B.; Borch, T. *Soil Syst.* **2018**, *2* (1), 14–19.
- (28) Brown, T. L.; Rice, J. A. *Anal. Chem.* **2000**, *72* (2), 384–390.
- (29) Dittmar, T.; Koch, B.; Hertkorn, N.; Kattner, G. *Limnol. Oceanogr.: Methods* **2008**, *6*, 230–235.
- (30) He, C.; Fang, Z.; Li, Y.; Jiang, C.; Zhao, S.; Xu, C.; Zhang, Y.; Shi, Q. *Environ. Sci. Process. Impacts* **2021**, *23*, 1466.
- (31) Li, Y.; Xu, C.; Chung, K. H.; Shi, Q. *Energy Fuels* **2015**, *29* (5), 2923–2930.
- (32) Hendrickson, C. L.; Quinn, J. P.; Kaiser, N. K.; Smith, D. F.; Blakney, G. T.; Chen, T.; Marshall, A. G.; Weisbrod, C. R.; Beu, S. C. *J. Am. Soc. Mass Spectrom.* **2015**, *26* (9), 1626–1632.
- (33) Smith, D. F.; Podgorski, D. C.; Rodgers, R. P.; Blakney, G. T.; Hendrickson, C. L. *Anal. Chem.* **2018**, *90* (3), 2041–2047.
- (34) Nelson, A. R.; Narrowe, A. B.; Rhoades, C. C.; Fegell, T. S.; Roth, H. K.; Chu, R. K.; Amundson, K. K.; Geonczy, S. E.; Young, R. B.; Steindorff, A. S.; Mondo, S. J.; Grigoriev, I. V.; Salamov, A.; Borch, T.; Wilkins, M. J. Playing with FiRE: A genome resolved view of the soil microbiome responses to high severity forest wildfire. *BioRxiv*, **2021**; DOI: 10.1101/2021.08.17.456416.
- (35) Emmett, M. R.; White, F. M.; Hendrickson, C. L.; Shi, D. H.; Marshall, A. G. *J. Am. Soc. Mass Spectrom.* **1998**, *9* (4), 333–340.
- (36) Xian, F.; Hendrickson, C. L.; Blakney, G. T.; Beu, S. C.; Marshall, A. G. *Anal. Chem.* **2010**, *82* (21), 8807–8812.
- (37) Savory, J. J.; Kaiser, N. K.; McKenna, A. M.; Xian, F.; Blakney, G. T.; Rodgers, R. P.; Hendrickson, C. L.; Marshall, A. G. *Anal. Chem.* **2011**, *83* (5), 1732–1736.
- (38) Corilo, Y. E. *PetroOrg Software*; Florida State University, Omics LLC: Tallahassee, FL, 2014.
- (39) Wapstra, A. H.; Audi, G.; Thibault, C. *Nucl. Phys. A* **2003**, *729* (1), 129–336.
- (40) Audi, G.; Bersillon, O.; Blachot, J.; Wapstra, A. H. *Nucl. Phys. A* **2003**, *729* (1), 3–128.
- (41) Mohr, P. J.; Taylor, B. N.; Newell, D. B. *RMP* **2008**, *80* (2), 633–730.
- (42) Marshall, A. G.; Rodgers, R. P. *Proc. Natl. Acad. Sci. U.S.A.* **2008**, *105* (47), 18090–18095.
- (43) Marshall, A. G.; Blakney, G. T.; Chen, T.; Kaiser, N. K.; McKenna, A. M.; Rodgers, R. P.; Ruddy, B. M.; Xian, F. *Mass Spectrometry* **2013**, *2* (Special\_Issue), S0009.
- (44) Senko, M. W.; Beu, S. C.; McLafferty, F. W. *American Society for Mass Spectrometry* **1995**, *6*, 52–56.
- (45) Kujawinski, E. B.; Freitas, M. A.; Zang, X.; Hatcher, P. G.; Green-Church, K. B.; Jones, R. B. *Org. Geochem.* **2002**, *33*, 171–180.
- (46) LaRowe, D. E.; van Cappellen, P. *Geochim. Cosmochim. Acta* **2011**, *75* (8), 2030–2042.
- (47) Hertkorn, N.; Frommberger, M.; Witt, M.; Koch, B. P.; Schmitt-Kopplin, P.; Perdue, E. M. *Anal. Chem.* **2008**, *80* (23), 8908–8919.
- (48) Kim, S.; Kramer, R. W.; Hatcher, P. G. *Anal. Chem.* **2003**, *75* (20), 5336–5344.

- (49) Rivas-Ubach, A.; Liu, Y.; Bianchi, T. S.; Tolić, N.; Jansson, C.; Paša-Tolić, L. *Anal. Chem.* **2018**, *90* (10), 6152–6160.
- (50) Smith, C. R.; Sleighter, R. L.; Hatcher, P. G.; Lee, J. W. *Environ. Sci. Technol.* **2013**, *47* (23), 13294–13302.